MEASUREMENT OF ANALYZING POWERS
FOR THE REACTION $\vec{p} + CH_2$ AT p_p = 1.75–5.3 GeV/c

L. S. Azhgirey, V. A. Arefiev, S. N. Basilev, Yu. P. Bushuev, V. V. Glagolev,
D. A. Kirillov, P. P. Korovin, P. K. Manyakov, N. M. Piskunov, I. M. Sitnik,
V. M. Slepnev

Joint Institute for Nuclear Research, Dubna, Moscow Region, Russia

J. Mušinský

Joint Institute for Nuclear Research, Dubna, Moscow Region, Russia
University of P. J. Šafárik, Jesenná 5, SK-04154 Košice, Slovak Republic

E. Tomasi-Gustafsson

DAPNIA/SPhN Saclay, Gif-sur-Yvette Cedex, France

L. Pentchev, C. F. Perdrisat

College of William and Mary, Williamsburg, USA

V. Punjabi

Norfolk State University, Norfolk, USA

M. K. Jones

TJNAF, Newport News, USA

G. F. Kumbartzki

Rutgers University, Piscataway, USA

I. Atanasov

Institute of Nuclear Research and Nuclear Energy BAS, Sofia, Bulgaria

Ажгирей Л. С. и др.   E1-2004-14

Измерения анализирующей способности реакции $\vec{p} + CH_2$
при $p_p = 1{,}75-5{,}3$ ГэВ/с

Мы представляем новые измерения анализирующей способности реакции $\vec{p} + CH_2 \rightarrow$ одна заряженная частица $+X$ при импульсах протонов 1,75; 3,8; 4,5 и 5,3 ГэВ/с. Эти результаты расширяют существующую базу данных, необходимых для протонной поляриметрии при промежуточных энергиях, и подтверждают жизнеспособность поляриметров с большим аксептансом, основанных на измерении этой реакции.

Работа выполнена в Лаборатории высоких энергий им. В. И. Векслера и А. М. Балдина ОИЯИ.

Azhgirey L. S. et al.   E1-2004-14

Measurement of Analyzing Powers for the Reaction $\vec{p} + CH_2$
at $p_p = 1.75-5.3$ GeV/c

We report a new measurement of analyzing powers for the reaction $\vec{p} + CH_2 \rightarrow$ one charged particle $+X$ at proton momenta of 1.75, 3.8, 4.5 and 5.3 GeV/c. These results extend the existing data basis, necessary for proton polarimetry at intermediate energy, and confirm the feasibility of a large acceptance polarimeter based on this process.

The investigation has been performed at the Veksler and Baldin Laboratory of High Energies, JINR.

INTRODUCTION

As all fundamental interactions are spin-dependent, the knowledge of polarization observables is essential for the understanding of the structure of hadrons and for disentangling the reaction mechanism in nuclear reactions. The polarization of intermediate energy protons (i.e., in the range from a few hundreds MeV to a few GeV) is generally measured with full azimuthal acceptance focal plane polarimeters; they measure the angular distribution of a charged particle issued from an inclusive reaction, usually the scattering from a carbon target [1] .

The availability of high luminosity polarized electron beams opens up the possibility to develop the experimental study of spin degrees of freedom in hadron physics at intermediate energy. In particular, a recent experiment at the Thomas Jefferson National Accelerator Laboratory [2], through the measurement of the recoil proton polarization in the elastic scattering of longitudinally polarized electrons on a proton target, showed that the ratio of the electromagnetic form factors of the proton, electric and magnetic, $G_{\mathrm{E}p}/G_{\mathrm{M}p}$, decreases monotonically with increasing four-momentum transfer squared, Q^2, starting at about 0.8 GeV^2 and up to 5.6 GeV^2, which corresponds to proton momenta up to 3.8 GeV/c. The extension of this measurement to larger momenta [3] requires the construction of a new polarimeter which will measure the polarization of recoil protons up to momenta of 5.7 GeV/c.

Polarization experiments are, in general, time consuming. Therefore a thorough optimization of the characteristics of the polarimeter is desired. This requires a careful study of the analyzing reaction, which has to have large yield and large analyzing powers. An optimization of the nature and the thickness of the polarimeter analyzer target as well as of the geometry of the detection system is required.

Complete angular distributions for the carbon analyzing power exist for values of proton momenta p_p between 0.644 and 1.92 GeV/c [1], between 1.75 and 3.2 GeV/c [4], using the direct polarized proton beam of the Saturne accelerator in Saclay, and for different thicknesses of the target. There are also data for different carbon target thickness, performed at ITEP in Moscow between 1.35 and 2.02 GeV/c [5].

Data on a 100 cm thick CH$_2$ target are available from Jefferson Laboratory, with polarized protons issued from $\vec{e}p$ elastic scattering [2]; there are also data at two angles at 4.45 GeV/c for a CH$_2$ target [6]. Analyzing powers on a thin proton

1

target are also available [7, 8]. The largest momentum for which the analyzing powers are known for pp scattering is 10 GeV/c [9].

The knowledge of the analyzing power for $\vec{p} + \mathrm{CH}_2$ reaction to the highest momentum of the proposed experiment, [3], is highly desirable to help planning the experiment. Such calibration has become possible at the Joint Institute for Nuclear Research (JINR) — Veksler–Baldin Laboratory of High Energy (VBLHE) accelerator complex where a polarized proton beam is available up to $p_p = 5.5$ GeV/c.

We report here new results at four beam momenta, $p_p = 1.75$, 3.8, 4.5 and 5.3 GeV/c, which extend the data base useful for proton polarimetry. Particular attention was devoted to the investigation of the optimal target thickness and of the useful angular range.

1. THE EXPERIMENT

The experiment was carried out with a slowly extracted beam of vector polarized deuterons produced by the POLARIS ion source [10] and accelerated by the Synchrophasotron at the VBLHE, JINR, Dubna.

1.1. The Beam. The intensity of the primary beam was up to $2 \cdot 10^9$ particles per beam spill. The beam structure consisted in a beam spill of 500 ms every 10 s. The vector deuteron polarization was flipped at each beam spill, one spill over three being unpolarized. This allowed a careful check of the experimental asymmetries.

The deuteron vector polarization, P_d, was periodically measured by two beam polarimeters, one at the exit of the source [11] and one after the extraction [12]. The polarization was different for the two beam polarization states. The following values were used in the analysis: $P^{(+)} = 0.612 \pm 0.037$ and $P^{(-)} = -0.568 \pm 0.037$, which correspond to the average values over the duration of the experiment. The asymmetry of the data itself allowed one to have a continuous on-line check of the eventual relative variations of the beam polarization.

The polarized protons were produced by fragmentation of the polarized deuteron beam on a 8 cm thick Be target, installed 60 m upstream of the polarimeter. Two dipoles of the beam transport line separated the break up protons at zero angle from the deuteron beam. The angular and momentum acceptances of the beam transport line are about $\Delta\Omega \simeq 10^{-4}$ sr and $\Delta p_p/p_p \simeq 3\%$, respectively [13]. Varying the primary beam intensity the average number of protons incident on the polarimeter target was kept at the level of $\simeq 2 \cdot 10^4$ per beam spill.

For the proton beam momentum of 5.3 GeV/c the deuteron beam momentum was 9 GeV/c. At this ratio of proton to deuteron momenta the polarization transfer from deuteron to proton is still equal to 1 [13,14]. For the other proton momenta

the corresponding deuteron beam momenta were twice as large as the proton momentum; hence, for the four proton momenta of this experiment the proton polarization was equal to the deuteron polarization.

1.2. The Detection. The POMME polarimeter, which has been widely used at Saclay, was transported to Dubna and used as a part of the detection system of the ALPHA spectrometer [15]. A detailed description of the polarimeter POMME can be found in [1].

A schematic view of the detection system is shown in Fig. 1, and the distances among the different elements are reported in Table 1.
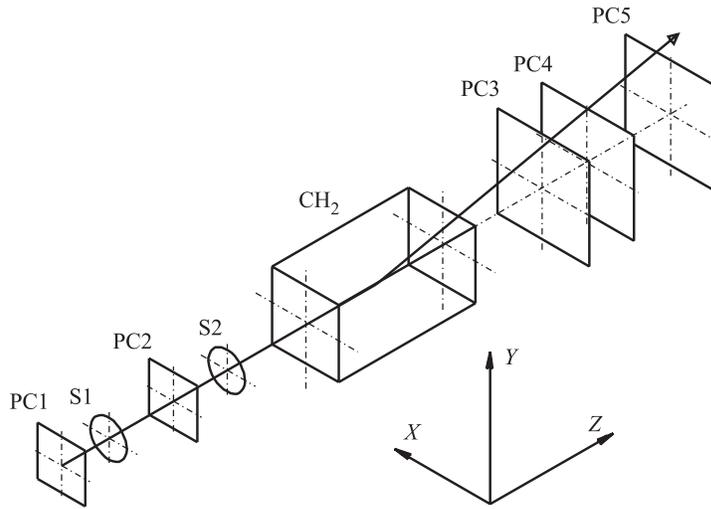
Fig. 1. Schematic view of the setup. S_i — scintillator counters, PC_i – proportional chambers

Table 1. **Detectors geometry and location. The origin is taken at the exit side of the target**

Detector	PC1	S1	PC2	S2	Target	PC3	PC4	PC5
Dimension [mm]	120×120	Ø 48	120×120	Ø 48		480×480	480×480	480×480
Location [mm]	–4970	–2630	–1250	–1075	0	110	325	800

The incident protons were detected by proportional chambers PC1, PC2 (ALPHA) with sensitive area 12×12 cm^2. The three wire chambers PC3–PC5 (POMME) with sensitive area 48×48 cm^2 were used to detect the trajectory of the charged particle after the scattering on the CH$_2$-analyzer. Each chamber has

x- and y-plane with wire spacing of 2 mm. The achieved plane angular resolution of the polarimeter was $\sigma_{\theta_x} = \sigma_{\theta_y} = 2.6$ mrad.

The trigger was given by the coincidence of signals from scintillation counters S1 and S2 of a diameter of 48 mm. The data acquisition system was able to record up to 4800 events per beam spill.

1.3. The Target. The polarimeter analyzer target consisted of several blocks of polyethylene of dimension $300 \times 300 \times 51$ mm^3 which could be assembled in variable sizes along the beam direction. The density of the material was $\rho = 0.919 \pm 0.002$ g/cm^2. The numbers of blocks used in the experiment were 8, 11, 14 and 17 (37.5, 51.6, 65.7, and 79.8 g/cm^2, respectively). For methodical studies, small statistics was collected with a thin target (5.1 g/cm^2, including scattering material of the polarimeter) at $p_p = 3.8$ GeV/c. To maximize angular acceptance, the geometry was such that the exit surface of the target was kept at a fixed point (taken as the origin of the reference system), as close as possible to the first rear chamber. As a result, the geometrical efficiency was 100 % up to scattering angles 9.2 and 10.6° for target thicknesses 79.8 and 37.5 g/cm^2, respectively.

2. THE DATA ANALYSIS

The number of events, for the inclusive reaction

$$\vec{p} + \mathrm{CH}_2 \rightarrow \text{one charged particle} + X, \tag{1}$$

is given by

$$N^{\pm}(\theta, \phi) = N_0(\theta) \left(1 + P_y^{(\pm)} A_y(\theta) \cos\phi \right), \tag{2}$$

where A_y is the analyzing power of the reaction and the sign $\pm$ refers to the spin orientation of the incident protons. The Laboratory coordinate system is shown in Fig. 1. The z-axis is along the beam direction, the y-axis is along the beam polarization (upwards) and the x-axis is such as to form a left-handed system. The polar angle θ is defined as the angle between the incident and the scattered trajectory. Due to the very narrow angular distribution of incident trajectories in the vertical plane (± 1 mrad) the y-axis can be considered as perpendicular to all incident trajectories, and ϕ is then the angle between the y-axis and the normal to the scattering plane. The convention is that $\phi = 0°$ for left scattering and $\phi = 90°$ for down scattering. $N_0(\theta)$ is the number of counts in some interval centered at θ for unpolarized beam.

The performance of a polarimeter is expressed in terms of the figure of merit, $\mathcal{F}$. For a given target thickness it is defined as

$$\mathcal{F}^2 = \int_{\theta} \frac{d\varepsilon}{d\theta} \, A_y^2(\theta) \, d\theta, \tag{3}$$

where the integration is done over the angular range where the polarimeter is efficient. In Eq. (3) $d\varepsilon/d\theta$ is the differential efficiency of the process, defined as the number of useful events emitted in the unit interval of θ, normalized to the number of incident particles, N_{inc}.

The knowledge of the figure of merit allows one to estimate the number of events, N_{inc}, necessary to obtain a given uncertainty in a polarization measurement. The statistical error in a measurement of the polarization, ΔP, can be expressed as

$$\Delta P = \sqrt{\frac{2}{N_{\mathrm{inc}}\mathcal{F}^2}}. \tag{4}$$

We will discuss the results in terms of transverse momentum p_t, instead of scattering angle, because, as it is shown below, this variable allows an easier comparison of the data for different beam momenta.

2.1. Collection of Data. The coordinates in the xz and yz planes allow one to find the parameters of the incident and scattered trajectories. The distance of closest approach is then calculated as the distance along a line perpendicular to both trajectories. The interaction vertex is the middle point of this segment.

At least two planes in the rear chambers had to fire, in order to collect events into statistics. For $p_t < 0.3$ GeV/c the presence of the first and third chambers was required. In order to suppress accidental events, further conditions were applied: the distance of closest approach had to be smaller than 50 mm; the z-coordinate of the interaction point had to be within the target edges plus 10 mm/θ (where θ is in radians).

The variable p_t was calculated taking into account energy losses inside the target:

$$E = E_p - \frac{dE}{dx}\rho z_{ps}, \quad p = \sqrt{E^2 - m_p^2}, \quad p_t = p\sin\theta, \tag{5}$$

where E_p is the energy of the incident beam, z_{ps} is the distance between the front edge of the target and the z-coordinate of the interaction point, ρ is the density of the target material, $dE/dx = 2.076$ MeV cm^2/g [16]. Averaged values of p, $\langle p_p \rangle$, were collected for each data set.

To compare the angular spectra for different experimental conditions, a Monte Carlo simulation of the geometrical efficiency was performed. The efficiency becomes lower than 100 % starting from p_t equal to 0.55, 0.7 and 0.85 GeV/c for beam momenta 3.8, 4.5 and 5.3 GeV/c, respectively. At $p_t = 1$ GeV/c the geometrical efficiency was 0.63, 0.93 and 0.98, for beam momenta 3.8, 4.5 and 5.3 GeV/c, respectively. All spectra, presented in this work, are divided by the angular efficiency functions.

2.2. The Efficiency. The absorption of the primary beam as a function of the thickness z of a target material is given by the expression:

$$\varepsilon_0(z) = \frac{N_0(z)}{N_0(0)} = e^{-z/\lambda_T}, \tag{6}$$

where N_0 is the number of unscattered particles and λ_T is the nuclear collision length.

In [18] it was shown that taking into account the rescattering effects leads to the expression for the integral efficiency:

$$\varepsilon = \int_{p_t} \frac{d\varepsilon}{dp_t} dp_t = (e^{z/\lambda_p} - 1)e^{-z/\lambda_T}, \tag{7}$$

where λ_p is the collision length for the process considered ($\lambda_p > \lambda_T$). The above expression holds when the emitted particle is identical to the incoming one. Keeping in mind that λ_T is known, the value of λ_p can be found as a solution of Eq. (7) using the experimental value of $\varepsilon(L)$ for each of the target thicknesses L.

When the target is thick, due to sizeable multiple scattering, in the region $0 < p_t < 0.1$ GeV/c the contributions of unscattered and scattered outgoing beams are overlapping. To disentangle these contributions, the experimental spectra, normalized to the number of good tracks in front chambers, were approximated by a function which is the sum of six gaussians in cylindrical coordinates:

$$\frac{d\varepsilon_0}{dp_t} + \frac{d\varepsilon}{dp_t} = \frac{1}{k} \ p_t \left(a_1 \exp(-b_1 p_t^2) + \sum_{i=2}^{6} a_i \ \exp(-b_i p_t^2) \right), \tag{8}$$

where k is efficiency of the block of rear chambers. It was assumed that the first gaussian describes the unscattered beam (convolution of multiple scattering and polarimeter angle resolution) and the other gaussians describe the distribution of scattered events. The typical value of χ^2 per number of degrees of freedom (NDF) for each beam momentum and target of thickness 1.1.

The value of k can be found from the condition

$$\varepsilon_0 = \frac{1}{k} \int a_1 \exp(-b_1 p_t^2) dp_t, \tag{9}$$

where ε_0 is defined in (6). The values of the integrals in (9) at $p_p = 3.8$ GeV/c are plotted in Fig. 2, a versus the target thickness, including the thin target measurement. The fit of these data by the function (6) multiplied by a free parameter k, gives $k = 0.655 \pm 0.031$ and $\lambda_T^{\text{exp}} = (53.5 \pm 2.3)$ g/cm^2. The latter number is in agreement with the observed variation of λ_T from 50.6 g/cm^2 at 1.55 GeV/c [17]
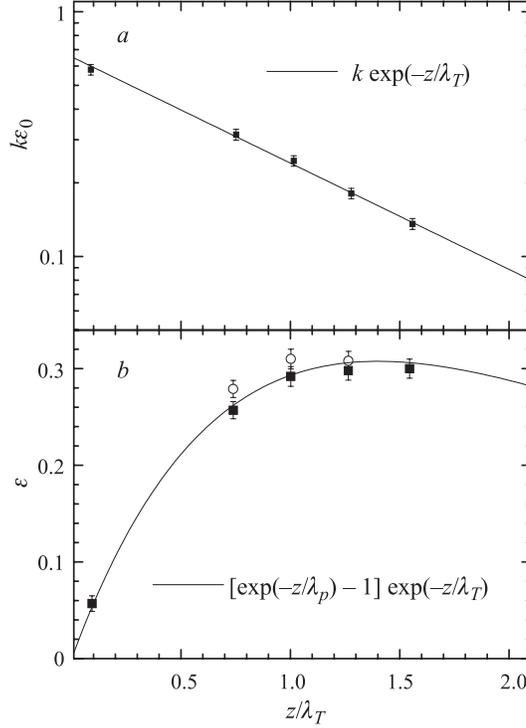
Fig. 2. z-dependence at $p_p = 3.8$ GeV/c: *a*) of the absorption for the unscattered beam; *b*) of the integral efficiency ε

to 57.0 g/cm^2 at momenta higher than 30 GeV/c [16], which validates the procedure chosen to split the spectra into scattered and unscattered parts.

The analysis of the fit data shows that the contribution of the unscattered events is lower than 5% for $p_t \geq 0.052$, 0.060, 0.067 and 0.077 GeV/c for target of thicknesses 37.5, 51.6, 65.7, and 79.8 g/cm^2, respectively. These values represent the lowest thresholds (LT) for the extraction of the analyzing power and do not depend on the beam momentum because the average multiple scattering angle is inversely proportional to the beam momentum.

The integral values for the scattered part of the beam along p_t from 0.08 (LT for the thickest target) up to 1 GeV/c for different target thicknesses are plotted in Fig. 2, *b* (solid points). The curve shown in this figure is the function (7) with λ_p, found for the data set with 37.5 g/cm^2 ($\lambda_T/\lambda_p = 0.58$). Its good agreement with experimental points at other values of L is evidence that the outgoing particles are mostly protons. Open points in this figure are integral values from the individual LT for each target thickness.

7

The differential efficiencies are plotted in Fig. 3 versus p_t, for different target thicknesses at $p_p = 3.8$ GeV/c. In Fig. 3, a, in the region $0 < p_t < 0.2$ GeV/c,
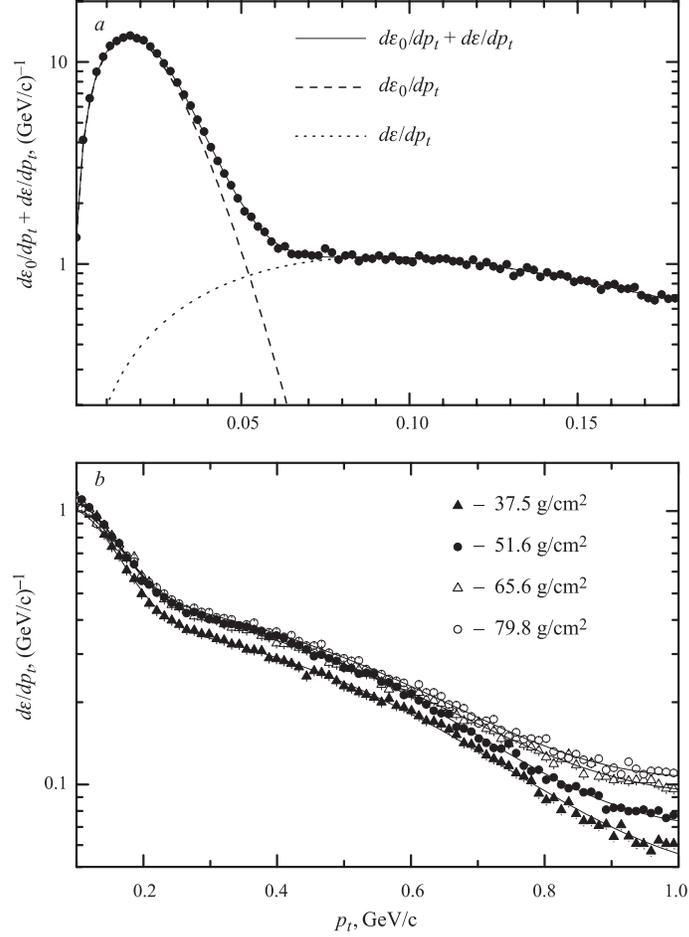
Fig. 3. The differential efficiency for different target thicknesses at 3.8 GeV/c. The spectrum at small p_t and its different components are shown in panel (a) for $L = 51.6$ g/cm^2. Panel (b) emphasizes the higher part of the spectra for $L = 37.5$ g/cm^2 (solid triangles), $L = 51.6$ g/cm^2 (solid circles), $L = 65.7$ g/cm^2(open triangles), and $L = 79.8$ g/cm^2 (open circles)

the description of data at $z = 51.6$ g/cm^2 is shown. The unscattered(scattered) component (see Eq. (8)) is reported as dashed(dotted) line and the sum as solid line. In Fig. 3, b the differential efficiency in the region, where the unscattered

8

component becomes negligible ($p_t > 0.1$ GeV/c), is shown for all target thicknesses, used in the experiment. For $p_t \geq 0.6$ GeV/c, the differential efficiency is larger when the target is thicker. As it is generally expected (and was shown numerically in [18]), the contribution of secondary reactions, which increases with target thickness, dominates in this region of p_t.

2.3. The Analyzing Powers. The scattered events were classified in 30 bins of the azimuthal scattering angle ϕ in the range $0 \div 2\pi$, and a number of bins of the transverse momentum transfer, p_t, depending on experimental conditions as summarized in Table 4.

Table 2. Analyzing power at different target thickness at $p_p = 3.8$ GeV/c

p_t	$A_y \pm \Delta A_y$			
	$L = 37.5$ g/cm^2	$L = 51.6$ g/cm^2	$L = 65.7$ g/cm^2	$L = 79.8$ g/cm^2
0.108	0.060± 0.014	0.054± 0.013	0.044± 0.012	0.077± 0.013
0.175	0.092± 0.016	0.107± 0.015	0.071± 0.013	0.095± 0.014
0.259	0.090± 0.014	0.091± 0.013	0.105± 0.013	0.091± 0.012
0.359	0.094± 0.014	0.110± 0.013	0.107± 0.013	0.111± 0.012
0.475	0.094± 0.015	0.096± 0.014	0.122± 0.013	0.083± 0.012
0.608	0.066± 0.016	0.090± 0.015	0.069± 0.014	0.084± 0.013
0.756	0.073± 0.019	0.085± 0.018	0.040± 0.016	0.059± 0.015
0.922	0.015± 0.026	0.039± 0.023	0.030± 0.020	0.018± 0.019
1.103	0.038± 0.033	0.025± 0.031	0.045± 0.025	0.025± 0.023

Table 3. **Values of maxima of curves fitting the data for different target thicknesses at $p_p = 3.8$ GeV/c**

$\langle p_p \rangle$, GeV/c	L_{CH_2} (g/cm^2)	$A_y^{max} \pm \Delta A_y^{max}$
3.76	37.5	0.103±0.007
3.74	51.6	0.113±0.007
3.72	65.7	0.107±0.006
3.71	79.8	0.109±0.006

From Eq. (2) it follows that the analyzing powers can be found, for each bin in p_t, from a linear fit of $R(p_t, \phi)$ as a function of $\cos\phi$, where

$$R(p_t, \phi) = \frac{N^+(p_t, \phi) - N^-(p_t, \phi)}{N^-(p_t, \phi)P^{(+)} - N^+(p_t, \phi)P^{(-)}} \qquad (10)$$

with statistical error

$$\Delta R(p_t, \phi) = \frac{1}{\langle P_y \rangle} \sqrt{\frac{4N^+(p_t, \phi)N^-(p_t, \phi)}{[N^+(p_t, \phi) + N^-(p_t, \phi)]^3}}, \qquad (11)$$

9

where $\langle P_y \rangle = (P^{(+)} - P^{(-)})/2$. The main source of systematic error comes from the precision with which the beam polarization is known:

$$\Delta A_y^{syst} = |A_y| \frac{\Delta \langle P_y \rangle}{\langle P_y \rangle},$$ (12)

where $\Delta \langle P_y \rangle / \langle P_y \rangle = 0.04$, including both statistical and systematic errors of beam polarization measurement. There is also a source of systematic errors for 5.3 GeV/c, due to assumption $P_p = P_d$.

Table 4. Analyzing power for different beam momenta

p_p (GeV/c)	p_t (GeV/c)	$\langle\theta\rangle$ (deg)	A_y	p_p	p_t	$\langle\theta\rangle$	A_y
1.75	$0.080 - 0.139$	3.66	0.186 ± 0.047	4.5	$0.151 - 0.227$	2.41	0.058 ± 0.015
	$0.139 - 0.215$	5.93	0.186 ± 0.032		$0.227 - 0.319$	3.50	0.073 ± 0.015
	$0.215 - 0.307$	8.78	0.233 ± 0.033		$0.319 - 0.427$	4.79	0.091 ± 0.016
	$0.307 - 0.414$	12.17	0.215 ± 0.032		$0.427 - 0.550$	6.28	0.098 ± 0.016
	$0.414 - 0.539$	16.10	0.241 ± 0.038		$0.550 - 0.689$	7.97	0.054 ± 0.017
	$0.539 - 0.680$	20.61	0.154 ± 0.052		$0.689 - 0.844$	9.87	0.010 ± 0.017
					$0.844 - 1.01$	11.96	0.017 ± 0.018
3.8	$0.080 - 0.139$	1.66	0.058 ± 0.006		$1.01 - 1.20$	14.25	0.004 ± 0.022
	$0.139 - 0.214$	2.67	0.090 ± 0.007	5.3	$0.162 - 0.239$	2.18	0.060 ± 0.010
	$0.214 - 0.307$	3.98	0.098 ± 0.008		$0.239 - 0.331$	3.11	0.076 ± 0.010
	$0.307 - 0.414$	5.51	0.106 ± 0.006		$0.331 - 0.439$	4.20	0.062 ± 0.011
	$0.414 - 0.539$	7.30	0.100 ± 0.008		$0.439 - 0.561$	5.47	0.086 ± 0.011
	$0.539 - 0.680$	9.34	0.078 ± 0.008		$0.561 - 0.698$	6.90	0.032 ± 0.012
	$0.680 - 0.837$	11.61	0.064 ± 0.011		$0.698 - 0.851$	8.49	0.033 ± 0.013
	$0.837 - 1.01$	14.15	0.023 ± 0.012		$0.851 - 1.02$	10.23	0.043 ± 0.014
	$1.01 - 1.20$	16.94	0.038 ± 0.015		$1.02 - 1.20$	12.15	0.026 ± 0.016

The analyzing powers for different target thicknesses at $p_p = 3.8$ GeV/c are given in Table 2 and in Fig. 4, a. The shape and the absolute value are very similar for the 4 thicknesses, and no systematic difference appears among the different sets of data. For each target thickness L_i, the analyzing powers at $p_p = 3.8$ GeV/c were fitted by a polynomial of 4th degree:

$$A_y^{L_i}(p_t) = c_i \sum_{j=1}^{4} d_j p_t^j.$$ (13)

The same coefficients d_j, $j = 1, 4$ reproduced all the data; only the normalization, c_i, was allowed to vary for the different targets. The result of the fit gives χ^2/NDF=0.78. The maxima of these polynomials are reported in Table 3. Fitting these maxima with a constant gives χ^2/NDF=0.40, which means that, within the error bars, the analyzing powers do not depend on the target thickness.

Therefore in Fig. 4, b and in Table 4 we report the data at each energy, summed over the target thicknesses. The average scattering angle $\langle\theta\rangle$ is calculated as $\langle\theta\rangle = \arcsin(p_t/\langle p_p\rangle)$.
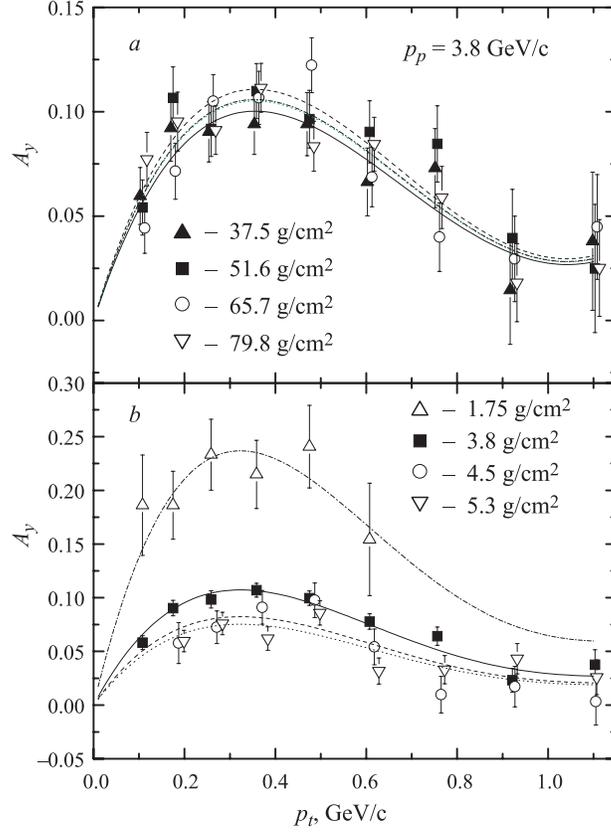
Fig. 4. Analyzing powers as a function of p_t: a) for different target thicknesses at $p_p = 3.8$ GeV/c; b) for different momenta at $L = 51.6$ g/cm^2

The data at the other two energies were also fitted by the polynomial of Eq. (13). The maxima of these functions, A_y^{max}, are given in Table 5.

In order to compare the analyzing powers on CH$_2$ and carbon targets, we performed a similar fit of the existing data on carbon [4, 5], based on a five degrees polynomial in Eq. (13). The set of data [5] at the lowest momentum, $p_p = 1.36$ GeV/c, was not included in this fit, because it follows essentially another law. In Table 5 we report the maxima of the best fit functions. When the

11

position of maximum is the same, such values allow one to estimate the energy dependence of the analyzing powers. The results for CH_2- and C-sets of data show inverse proportionality to $p_{lab} = \langle p_p \rangle$, as is shown in Fig. 5. Therefore, the analyzing powers for C- and CH_2-targets can be parametrized as:

$$A_y(p_t, p_{lab}) = \frac{\sum_{j=1}^{m} d_j p_t^j}{p_{lab}}. \tag{14}$$

The results of the fit are given in Table 6. In columns p_t^{max}, A_y^{max} the positions and values of maximum of function (14) at $p_{lab} = 1$ GeV/c for C- and CH_2-targets are given. The ratio of these values shows that the analyzing powers on a CH_2-target are larger by $\simeq 12\,\%$ compared to a C-target.

Table 5. Values of maxima of the best fit functions. The carbon data are taken from [4,5]

p_p (GeV/c)	$\langle p_p \rangle$	L_{CH_2} (g/cm^2)	A_y^{max}
1.75	1.69	37.5	0.237±0.017
3.8	3.73	$\langle 58.9 \rangle$	0.108±0.003
4.5	4.44	$\langle 57.0 \rangle$	0.085±0.009
5.3	5.22	$\langle 69.9 \rangle$	0.076±0.006
T_p [GeV]		L_C (g/cm^2)	
1.05	1.70	53	0.215 ± 0.003
1.35	2.03		0.185 ± 0.004
1.60	2.31		0.140 ± 0.005
1.80	2.52		0.130 ± 0.004
2.00	2.73		0.131 ± 0.005
2.24	2.98		0.120 ± 0.005
2.40	3.15		0.109 ± 0.006
p_p [GeV/c]			
1.60	1.58	19.4	0.221 ± 0.005
	1.56	36.5	0.230 ± 0.006
1.78	1.76	19.4	0.208 ± 0.005
	1.74	36.5	0.203 ± 0.004
2.02	2.00	19.4	0.179 ± 0.004
	1.98	36.5	0.173 ± 0.005

Table 6. Best fit parameters for CH_2- and C-data

Target	d_1	d_2	d_3	d_4	d_5	p_t^{max} GeV/c	A_y^{max}	χ^2/NDF
CH_2	3.02± 0.13	−7.33±0.66	6.17±1.11	−1.74±0.59	0.	0.318	0.398	0.94
C	3.48±0.08	−12.14±0.64	18.9±1.6	−14.2±0.16	4.10±0.54	0.281	0.357	1.31

12
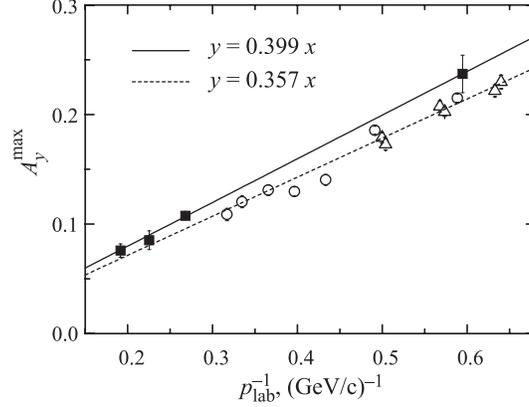
Fig. 5. Momentum dependence of CH_2- and C-data. Solid squares – current data, open circles – [4], open triangles – [5]. Solid line – fit of CH_2-data, dashed line – fit of C-data

2.4. The Figure of Merit. Based on the approximation of the efficiency (8), individual for each set of data, and analyzing power (13) (common for each beam momentum) we can calculate the figure of merit for an ideal apparatus (100 % efficiency, high angular resolution). In Fig. 6 we present the figure of merit calculated as the integral

$$\mathcal{F}^2(p_t) = \int_{a(L)}^{p_t} A_y^2(p_t') \frac{d\varepsilon}{dp_t'} dp_t', \qquad (15)$$

where $a(L)$ is LT for each target thickness. Such integral representation allows one to estimate the contribution to the figure of merit from different regions of p_t. As an example, at $L = 51.6$ g/cm^2

$$\mathcal{F}^2(0.06 < p_t < 0.2) \simeq \mathcal{F}^2(0.4 < p_t < 1.0),$$

and this relation does not depend on energy. Therefore high angular resolution of the polarimeter allows one to collect statistics from LT, and it is a very important feature for polarimetry at high energies. On the other hand, increasing the target thickness over the nuclear collision length or the polarimeter acceptance above $p_t \simeq 0.7$ GeV/c, does not improve the figure of merit.

3. CONCLUSIONS

We measured the analyzing power for the inclusive reaction $\vec{p} + CH_2 \rightarrow$ one charged particle $+X$, at proton momenta of 3.8, 4.5 and 5.3 GeV/c, for

13

different thicknesses of the CH_2-target, and at proton momentum 1.75 GeV/c, with a 37.5 g/cm^2 thick target.
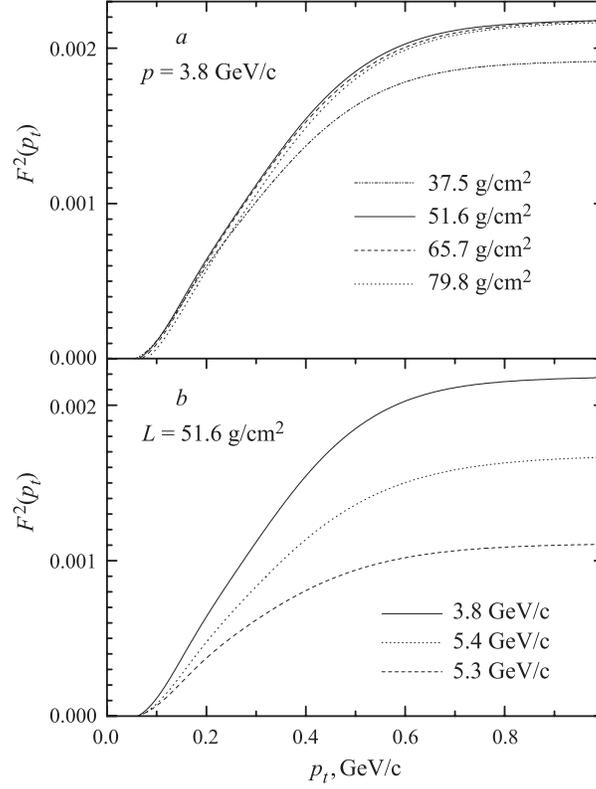
Fig. 6. Figure of merit as a function of p_t: *a*) for different target thicknesses at $p_p = 3.8$ GeV/c; *b*) for different momenta at $L = 51.6$ g/cm^2

The results show the following interesting features.

- For protons of 3.8 GeV/c, the analyzing power is fairly independent from the amount of material in the analyzer, from 37 to 80 g/cm^2.

- Target thickness above nuclear collision length and the polarimeter acceptance above $p_t > 0.7$ GeV/c do not improve figure of merit.

- The analyzing power decreases with increasing incident momentum, but it is still sizeable at a proton momentum of 5.3 GeV/c.

14

- The CH_2 shows a larger analyzing power than the carbon.

- In a wide region of proton momenta, the analyzing power both for carbon and CH_2-targets has a maximum around $p_t = p \sin\theta \simeq 0.3$ GeV/c.

- High angular resolution of the polarimeter is very important to increase the figure of merit.

- In the momentum range of interest here, the analyzing power is inversely proportional to the incident momentum.

ACKNOWLEDGMENTS

REFERENCES

1. B. Bonin et al., Nucl. Instr. and Meth. A288, 379 (1991);
   E. Tomasi-Gustafsson, POMME Manual, LNS/Ph/92-07.

2. M.K. Jones et al., Phys. Rev. Lett. **84**, 1398 (2000);
   O.Gayou et al., Phys. Rev. Lett. **88**, 092301 (2002);
   O. Gayou, thesis College of William and Mary, (2002), unpublished.

3. Proposal to JLab PAC20: 'Measurement of G_{Ep}/G_{Mp} to $Q^2 = 9$ GeV^2 via Recoil Polarization', (Spokepersons: C.F. Perdrisat, V. Punjabi, M.K. Jones and E. Brash), JLab, July 2001.

4. N.E. Cheung et al., Nucl. Instr. & Meth., A **363**, 561 (1995).

5. I.G. Alekseev et al., Nucl. Instr. & Meth., A **434**, 254 (1999).

6. E.V. Anoshina et al., Phys. of Atomic Nuclei, **60**, 224 (1997).

7. J.H. Parry et al., Phys. Rev. D **8**, 45 (1973).

8. M. Altmeier et al. [EDDA Collaboration], Phys. Rev. Lett. **85**, 1819 (2000).

9. D. Miller et al., Phys. Rev. D **16**, 2016 (1977);
   R. Diebold et al. Phys. Rev. Lett. **35**, 632 (1975).

10. N.G. Anishchenko et al., in: Proc. of 5th Int. Symp. on High Energy Spin Physics (Brookhaven, 1982), AIP Conf. Proc. 95, 445 (1983).

11. Yu.K. Pilipenko, V.M. Slepnev, L.S. Zolin, in: Proc. of 14th Int. Spin Phys. Symp., Osaka, Oct. 16-21, 2000. Ed. by K. Hatanaka, T. Nakano, K. Imai, H. Ejiri, 0-7354-0008-3.

12. L.S. Azhgirey et al., PTE **1**, 51 (1997), transl. in Instrum. and. Exp. Technics **40** (1997) 43; L.S. Azhgirey et al., Nucl. Instr. & Meth. A497, 340 (2003).

13. B. Kuehn et al., Phys. Lett. B **334**, 298 (1994);
    A.A. Nomofilov et al., Phys. Lett. B **325**, 327 (1994);
    L.S. Azhgirey et al., JINR Rapid Com. No. 3[77]-96, 23 (1996).

14. V. Punjabi et al., Phys. Lett. B **350**, 178 (1995).

15. V.G. Ableev et al., PTE **3**, 63 (1978).

16. D.E. Groom et al., Eur. Phys. J. **C 15**, 1 (2000).

17. J. Jaros et al., Phys. Rev. C **18**, 2273 (1978).

18. I.M. Sitnik in: Proc. of IX Workshop on High En. Spin Phys., Dubna Aug. 2-7, 2001, Ed. by A.V. Efremov, O.B.Teryaev, Dubna, 2002; preprint JINR E13-2003-61, submitted to Nucl. Instr. & Meth. A.